Fast preparation route to high-performances textured Sr-doped $Ca_3Co_4O_9$ thermoelectric materials through precursor powder modification

M. A. Torres,[1] G. García[2], I. Urrutibeascoa[3], M. A. Madre,[1,*] J. C. Diez,[1] A. Sotelo[1]

[1]ICMA (CSIC-Universidad de Zaragoza), C/María de Luna 3, 50018-Zaragoza (Spain).

[2]Centro Stirling S. Coop., 20550, Aretxabaleta (Guipuzcoa), Spain

[3]Mondragon Unibertsitatea, 20500, Arrasate (Guipuzcoa), Spain

Abstract

This work presents a short and very efficient preparation method to produce high performance textured $Ca_3Co_4O_9$ thermoelectric materials through initial powders modification. Different samples were prepared by hot uniaxial pressing from powders obtained by the classical solid state method, and by attrition milling. Microstructure has shown good grain orientation, and low porosity in both cases, while slightly lower grain sizes were obtained in samples prepared from attrition milled powders. Density measurements confirmed the high density of all samples (around 96 % of the theoretical). These similar characteristics are reflected in, approximately, the same electrical resistivity and Seebeck coefficient values for both types of samples. However, in spite of similar PF value at low temperatures, it is slightly higher at high temperature for the attrition milled samples. On the other hand, the processing time reduction (from 38, to 2 h) when using attrition milled precursors, leads to lower mechanical properties in these samples. All these data clearly point out to the similar characteristics of both kinds of samples, with a drastic processing time decrease when using attrition milled precursors, which is of the main economic importance when considering their industrial production.

Keywords: Ceramics; Oxides; Hot-pressing; Electrical properties; Power factor

* Corresponding author: M. A. Madre (amadre@unizar.es). ICMA (CSIC-Universidad de Zaragoza), C/María de Luna 3, 50018-Zaragoza (Spain). Fax: +34 976761957; Tel.: +34 976762617

1. Introduction

In the last decades, fossil fuels energy consumption has been drastically raised, with the corresponding increase of CO_2 and greenhouse gases emissions. Moreover, the relatively low efficiency of energy transforming systems leads to large energy losses in form of heat. In this situation, thermoelectric (TE) materials can play an important role as they can transform the wasted heat from different sources (power plants, automobiles, etc.) to useful electric power through the Seebeck effect [1]. The performances of these materials are evaluated through their figure-of-merit:

$$ZT = \frac{S^2 T}{\rho \kappa}$$

where S is the Seebeck coefficient; T, absolute temperature; ρ, electrical resistivity; and κ, thermal conductivity [2].

Even if thermoelectric materials are known for long time, they are rarely used in practical applications. At present, commercial devices are mostly applied for refrigeration purposes and are built using intermetallic legs, as Bi_2Te_3 or $CoSb_3$ [3,4]. When used as energy generators, in spite of their relatively high performances, they have a relatively low maximum working temperature. This is due to a possible degradation or sublimation of heavy metals when these materials are subjected to relatively high temperatures under air. The problems associated with temperature were surpassed when promising high temperature thermoelectric performances were discovered in $Na_2Co_2O_4$ ceramic [5]. Moreover, the high working temperature of this material is beneficial for energy conversion by harvesting wasted heat in high temperature processes. Consequently, a broad research field on thermoelectric oxides has been opened from this moment, leading to the discovery and improvement of

several families, as CoO- (*p*-type), TiO-, or MnO-based (*n*-type) ones [6-12]. Among the cobaltites, the $Ca_3Co_4O_9$ (349) material is one of the most promising *p*-type ones, not only by their relatively high performances, but also due to the absence of heavy metals. On the other hand, the anisotropy of its crystal structure [6] leads to strongly anisotropic properties, opening a window for their improvement through different grain alignment techniques [13-17]. Among these techniques, the hot-pressing process [14] is one of the most easily scalable for industrial production. Nevertheless, the typical solid-state process used to produce these materials is too long to be economically suitable. The aim of this work is producing textured 349 materials with the closest possible performances to the obtained through the classical ceramic route (used as reference) using a fast and efficient processing route via precursor powders modification using attrition milling. These modifications can produce, from the economic point of view, more attractive materials for industrial production. The precursor powders evolution will be studied and will be related with the final microstructure, and mechanical and thermoelectric properties.

Hereafter, samples produced from the classically solid state prepared precursors will be named CS, and the ones from attrition milled precursors, AT.

2. Experimental

Taking into account the improvements produced in previous works by Sr-doping in 349 sintered materials [18,19], the initial stoichiometry used in this work has been $Ca_{2.93}Sr_{0.07}Co_4O_9$. All the samples have been prepared using $CaCO_3$ (≥ 99 %, Aldrich), $SrCO_3$ (≥ 98%, Aldrich), and CoO (99.99 %, Aldrich) commercial powders. They were

weighed in the appropriate amounts, mixed and milled for 30 min in water medium using an agate ball mill for the classical solid-state method, and an attrition mill for the fast processing route. Both slurries were then rapidly dried under infrared radiation until total water evaporation. The resulting powders were subsequently manually milled to break the agglomerates, followed by a calcination process. For the classical solid-state route, the powders were subjected to a two-step thermal treatment, at 750 and 800 ºC for 12 h with an intermediate manual milling, as previously reported [18]. On the other hand, the powders obtained through attrition milling were calcined at temperatures ranging between 800 and 850 ºC for 1 h. After thermal treatments, in both cases, the black powders were cold uniaxially pressed at 250 MPa in form of discs. The CS green ceramics were hot uniaxially pressed in the optimal conditions experimentally determined, 850 ºC and 30 MPa for 14 h, while the AT samples were processed at temperatures between 800 and 850 ºC and pressures ranging from 30 to 50 MPa for 1 h. Finally, the hot-pressed samples were cut with on pieces for their subsequent characterization.

The precursor powders were studied before and after thermal treatments using a Field Emission Scanning Electron Microscope at 5 and 10 kV (FESEM, Carl Zeiss Merlin) to determine their microstructural evolution. FTIR spectroscopy has been performed on thermally treated powdered samples in a Bruker IFS 28 Spectrometer in ATR mode between 700 and 1800 cm^{-1}, to assess the calcium and strontium carbonates decomposition. Hot uniaxially pressed samples have been microstructurally studied on representative polished longitudinal sections and transversal fractures in a FESEM at 20 kV with attached EDS system to qualitatively determine the chemical composition of

the different phases. Phase identification in the textured samples has been made on powders using X-ray diffraction (XRD) in a PANalytical X'Pert MPD Philips diffractometer at 40 kV and 30 mA, with 2θ between 5 and 40 º. Density values have been determined through the Archimedes' method, taking 4.677 g cm^{-3} as the theoretical one [6]. At least five samples of each preparation procedure were measured three times to minimize measurement errors. Mechanical properties of the different samples were evaluated using the three point bending test in an Instron 5565 machine with a 10 mm loading span fixture and a punch displacement speed of 30 μm/min on, at least, five specimens of each experimental condition. Samples where around 3 mm x 3 mm section and 15 mm length, and were tested in the parallel direction to the applied pressure for the texturing process.

Electrical resistivity and Seebeck coefficient were simultaneously measured in a LSR-3 system (Linseis GmbH) by the four-probe DC technique in the steady state mode between 50 and 800 ºC. Measured samples were about 3 mm x 3 mm section and 12 mm length, and they were measured in the perpendicular direction to the applied pressure for the hot-pressing process. With these data, power factor ($PF = S^2/\rho$) of all samples was calculated to determine their performances.

3. Results and discussion

3.1. Precursors

Fig. 1a shows the image of $CaCO_3$, $SrCO_3$, and CoO precursors mixture. In the micrograph, the small grains have been associated to CoO, while the platelike ones correspond to $CaCO_3$, probably accompanied by $SrCO_3$. On the other hand, Figs. 1b,

and c present representative micrographs of this mixture after ball, and attrition milling, respectively. Despite using the same initial powders in both cases, the micrographs clearly show significant differences in grain sizes after the milling processes. As it can be clearly seen in the pictures, the CS mixtures are mainly composed of relatively large grains (> 1 μm) accompanied of smaller ones. This size distribution can be associated to the different hardness of each initial compound, which produces different size reduction. On the other hand, even if AT powders maintain similar distribution, the largest grains are around 200 nm, clearly showing a drastic decrease of their sizes. This is an important effect taking into account that the reactivity of these powders should be increased when their sizes are decreased.

Fig. 2 show the FTIR spectra performed on the initial mixture, and after the calcination procedure. As it can be observed in the graph, the carbonates can be easily identified in the initial mixture (Fig. 2a), through the bands centered at 1450-1410 (strong), and 880-860 cm^{-1} (medium) [20]. After calcination, only a small amount of carbonates is present in the CS precursors (Fig. 2b), while a satellite peak at around 1380 cm^{-1} appears, and can be associated to humidity, as it corresponds to the bending mode of O-H bond (1420-1330 cm^{-1}), and confirmed by the absorbance band appearing at 1650-1600 cm^{-1} [21]. On the other hand, in spite of the higher reactivity of AT powders and the higher calcination temperatures, the very short time leads to higher carbonate content in samples treated at 800, and 825 ºC, while the same spectrum obtained in CS powders is recorded in the AT ones after 1 h at 850 ºC (see Figs. 2c-e). Consequently, the adequate calcination conditions of AT precursors have been fixed in 850 ºC for 1 h.

The microstructural modifications of precursor powders after calcination procedures are illustrated in Fig. 3, where representative micrographs are displayed. In this figure, it is easy to observe that despite the fast grain growth of AT powders, they are still much smaller than the CS ones, due to their different thermal treatments (750 and 800 ºC for 12 h each, and 850 ºC for 1 h, for CS, and AT powders, respectively). The average grain sizes for CS precursors are larger than 7 μm, while AT ones are only around 2 μm, even if still smaller grains can be found in this case due to the very short calcination process. EDS analysis performed in all powders has shown that the plate-like grains produced during the calcination correspond to the $Ca_3Co_4O_9$ phase. Consequently, it can be easily deduced that the very small grain sizes obtained through attrition milling is very advantageous to decrease calcination time, when compared with the necessary in the classical solid state method.

3.2. Textured materials

In spite of the different conditions used for texturing AT samples, for the sake of clarity only the results obtained in the best conditions (850 ºC and 50 MPa) will be discussed and compared with the obtained on the CS samples.

Fig. 4 presents the powder XRD patterns of textured samples. As it can be seen in the graph, most of the peaks (identified in the plot by their diffraction plane) can be associated to the $Ca_3Co_4O_9$ phase, as the major one [22] in both cases. On the other hand, minor peaks (indicated with * in Fig. 4a) corresponding to the $Ca_3Co_2O_6$ phase [22] can be observed in samples produced from CS precursors. The identification of this phase is very typical in the available literature [23], while it is not appearing in the AT

samples probably due to the higher homogeneity and lower grain sizes of the precursors mixture. Other possibilities to avoid the $Ca_3Co_2O_6$ phase presence is the addition of Co_3O_4 [24], which enhances the reaction to produce the $Ca_3Co_4O_9$ one. The presence of $Ca_3Co_2O_6$ phase in CS samples can be explained taking into account that the $Ca_3Co_4O_9$ phase formation is limited by the oxygen diffusion into the sample, and it is much slower when the grain sizes are larger.

Microstructural studies performed on longitudinal polished section of both samples have shown that they are very similar, with very small porosity, pointing out to a high densification of samples. The only significant difference has been found in CS materials, where the secondary $Ca_3Co_2O_6$ phase can be identified, as can be observed in the micrograph displayed in Fig. 5a (dark grey contrast shown by arrows), while the main phase is the $Ca_3Co_4O_9$ (grey contrast in both micrographs). This phase is not appearing in AT samples due to the higher homogeneity and reactivity of these precursors (see Fig. 5b). On the other hand, even if porosity observed in the picture seems to be relatively high, it should be highlighted that most of it has been formed by stripping the superficial grains. This effect is especially relevant in these textured materials owing to the grains shape and orientation, which preferentially align the weakly bonded planes parallel to the samples surface.

In order to confirm the low porosity of these samples, observed in the SEM micrographs, density has been determined in both types of samples. The mean values, together with their standard error, and their relative density, are presented in Table 1. As it can be easily observed, in spite of the different hot-pressing process duration, the densities of both samples are nearly the same, with no significant differences. This fact

is due to the lower sizes of AT precursors which allow enhancing the diffusion speed, rapidly decreasing the amount of porosity in these samples.

The effect of the different thermal treatment duration is also reflected in the microstructure obtained after the hot-pressing process. In Fig. 6, representative views of transversal fractured sections clearly illustrate that CS samples possess much larger grain sizes than the AT ones, in agreement with previous works [25]. Moreover, despite of the higher pressure applied on AT samples during the hot-pressing process, the grains orientation is very similar in both cases. Consequently, it can be deduced that the effect of the higher pressure is probably minimized by the shorter hot-pressing duration.

Mechanical properties, performed by three point bending tests, are summarized in Table 1. These results show that AT samples possess lower bending strength than the CS ones. Taking into account that the only significant differences between CS and AT textured materials were the presence of $Ca_3Co_2O_6$ secondary phase, and the larger grain sizes in CS samples, the lower mechanical performances exhibited by the AT materials can be explained by the very short hot-pressing process which hinders the formation of mechanically strong grain boundaries. Other feature observed in the table is the lower standard error obtained in AT samples, which points out to a higher homogeneity of these materials. These values are much higher than the reported in the literature for $Ca_3Co_4O_9$ obtained through a two-step sintering procedure (40 MPa), even with Ag additions (110 MPa) [26]. On the other hand, they are comparable to the already reported on hot uniaxially pressed $Ca_3Co_4O_9$ samples (250 MPa) [27]. In any case, it is clear that the values obtained in this work are enough for practical applications.

Electrical resistivity values, as a function of temperature, determined on the samples prepared through the different routes are displayed in Fig. 7. As it can be observed in the graph, they show very similar semiconducting-like behaviour ($d\rho/dT \leq 0$), and values in the whole measured temperature range. The minimum values at room temperature (RT), 8.3 mΩ cm, are lower than the reported for sintered specimens (15-30 mΩ cm) [13,18,28], or prepared through alternative methods (11-15 mΩ cm) [29-31]. Moreover, they are comparable to the reported in spark plasma sintered (SPS) materials (7-8 mΩ cm) [13,32,33]. When evaluating the high-temperature values determined in this work (5.7-5.9 mΩ cm) with the best reported in the literature, once again they are much lower than the determined in sintered materials or prepared via alternative methods (34-16.5, and 10-12.5 mΩ cm, respectively) [13,18,28-31]. Furthermore, they remain similar to the measured in SPS textured samples (6-7 mΩ cm) [13,32,33]. These values, clearly evidence that the materials prepared in this work possess well oriented grains and good electrical connectivity between them, independently of the preparation process. The fact that AT samples show very close resistivity values to those measured in CS ones, in spite of the mechanically weaker grain boundaries, is due to the lower grain sizes and higher reactivity of AT precursors. These characteristics promote cleaner grain boundaries (with lower resistivity) than the obtained in CS samples, compensating the higher number of grain boundaries in AT samples.

Fig. 8 shows the evolution of Seebeck coefficient as a function of temperature in both types of samples. The values are positive in the whole measured temperature range, indicating a predominant hole conduction mechanism. Moreover, the magnitude of S increases with temperature, in agreement with previously published data [18,28], in both

cases. At RT, S values are nearly the same, independently of the preparation route, indicating that both samples possess very similar charge carrier concentration, in agreement with Koshibae's expression [34]. On the other hand, at 800 ºC the AT samples show higher S values than the measured in CS ones. The fact that S is slightly higher for CS samples at room temperature can be due to the absence of $Ca_3Co_2O_6$ secondary phase in AT samples, as previously discussed. On the other hand, at high temperatures, AT samples show higher S values than CS ones due to their smaller grain sizes. This behavior can be explained taking into account that $Ca_3Co_4O_9$ phase is known to lose oxygen at high temperatures, decreasing the carrier concentration [35], and this process is faster when the number of grain boundaries is raised. When comparing the S highest values determined at room temperature and 800 ºC (145, and 205 $\mu V\ K^{-1}$, respectively), they are in the order of the reported for sintered, prepared through alternative methods or SPS (125-150, and 155-230 $\mu V\ K^{-1}$, at RT, and 800 ºC, respectively) [13,18,28-33].

The samples performances have been evaluated through their PF and presented, as a function of temperature, in Fig. 9. As it can be observed, PF is increased with temperature in both cases, being slightly higher for AT samples at high temperatures. The maximum values at 800 ºC (0.7 mW $K^{-2}\ m^{-1}$) are much higher than the best reported in textured materials prepared by SPS (0.45 mW $K^{-2}\ m^{-1}$) [32] or by alternative methods (0.44 mW $K^{-2}\ m^{-1}$) [30]. Consequently, they are among the highest obtained so far in bulk $Ca_3Co_4O_9$ polycrystalline materials reported so far in the best of our knowledge.

The previously discussed data evidence that precursor powder modification through attrition milling allows reaching equivalent performances to those obtained using ball milling, with the additional advantage of a very important processing time reduction. The thermal treatments duration to obtain the final bodies has been decreased from 38 h, in CS materials, to 2 h in AT ones. This is a very important result from the economic point of view, which can be of interest when considering the industrial production of these materials.

4. Conclusions

This work presents a very short and efficient preparation method to produce high performance textured $Ca_3Co_4O_9$ thermoelectric materials through initial powders modification. Different samples were prepared by hot uniaxial pressing using two different precursor powders, one of them obtained by ball milling, while the other has been produced through attrition milling. Microstructure of hot-pressed materials has shown good grain orientation and low porosity, in both cases. The most significant difference has been observed in the grain sizes, which are smaller in samples prepared from attrition milled powders. Density measurements confirmed the high density (around 96 % of the theoretical) of both kinds of samples. Mechanical properties, determined by three point bending tests, were lower for AT samples due to the short hot-pressing process which hinders the formation of very strong grain boundaries. Electrical resistivity and Seebeck coefficient are very similar in both cases, in the whole measured temperature range. However, in spite of a similar PF value at low temperatures, it is slightly higher in AT samples at high temperature. All these data clearly point out to the

similar characteristics of both kinds of samples, highlighting the additional advantage of attrition milling on the processing time reduction (from 38 to 2 h). This fact is of the main economic importance when considering the industrial production of these materials.

Acknowledgements

The authors wish to thank the Gobierno de Aragón-FEDER (Research Group T 54-17 R), the Spanish MINECO-FEDER (MAT2017-82183-C3-1-R), and the Basque Government Industry Department through the Elkartek program (Exp: KK-2017/00099 - HiTOM) for financial support. The use of Servicio General de Apoyo a la Investigación-SAI, Universidad de Zaragoza is also acknowledged.

Data availability

The raw/processed data required to reproduce these findings cannot be shared at this time as the data also forms part of an ongoing study.

Statement of responsibility

M. A. Torres, and A. Sotelo prepared the samples and evaluate densities. M. A. Madre, and J. C. Diez determined microstructural and thermoelectric properties. G. García, and I. Urrutibeascoa measured mechanical properties and characterize structural features. All authors collaborate equally on the manuscript preparation.

Disclosure of conflict of interest

No conflict of interest has to be declared.

References

1 Elsheikh MH, Shnawah DA, Sabri MFM, *et al.* A review on thermoelectric renewable energy: Principle parameters that affect their performance. Renew Sustain Energy Rev, 2014, 30: 337–355.

2 Rowe DM, Thermoelectrics handbook: macro to nano, CRC Press, Boca Raton, USA, 2006.

3 Wang H, Hwang J, Snedaker ML, *et al.* High Thermoelectric Performance of a Heterogeneous PbTe Nanocomposite. Chem Mater, 2015, 27: 944–949.

4 Santamaria JA, Alkorta J, Sevillano JG. Microcompression tests of single-crystalline and ultrafine grain Bi_2Te_3 thermoelectric material. J Mater Res, 2015, 30: 2593–2604.

5 Terasaki I, Sasago Y, Uchinokura K. Large thermoelectric power in $NaCo_2O_4$ single crystals. Phys Rev B, 1997, 56: 12685–12687.

6 Masset AC, Michel C, Maignan A, *et al.* Misfit-layered cobaltite with an anisotropic giant magnetoresistance: $Ca_3Co_4O_9$. Phys Rev B, 2000, 62: 166-175.

7 Madre MA, Rasekh Sh, Diez JC, *et al.* New solution method to produce high performance thermoelectric ceramics: A case study of Bi-Sr-Co-O. Mater Lett, 2010, 64: 2566–2568.

8 Wang H, Wang CL. Thermoelectric properties of Yb-doped $La_{0.1}Sr_{0.9}TiO_3$ ceramics at high temperature, Ceram Int, 2013, 39: 941–946.

9 Li LL, Liu YF, Qin XY, *et al.* Enhanced thermoelectric performance of highly dense and fine-grained $(Sr_{1-x}Gd_x)TiO_{3-\delta}$ ceramics synthesized by sol–gel process and spark plasma sintering. J Alloys Compds, 2014, 588: 562–567.

10 Zhu YH, Su WB, Liu J, *et al.* Effects of Dy and Yb co-doping on thermoelectric properties of $CaMnO_3$ ceramics. Ceram Int, 2015, 41: 1535–1539.

11 Sotelo A, Torres MA, Madre MA, *et al.* Effect of synthesis process on the densification, microstructure, and electrical properties of $Ca_{0.9}Yb_{0.1}MnO_3$ ceramics. Int J Appl Ceram Technol, 2017, 14: 1190–1196.

12 Lohnert R, Stelter M, Topfer, J. Evaluation of soft chemistry methods to synthesize Gd-doped $CaMnO_3$-delta with improved thermoelectric properties. Mater Sci Eng B, 2017, 223: 185–193.

13 Noudem JG, Kenfaui D, Chateigner D, *et al.* Granular and Lamellar Thermoelectric Oxides Consolidated by Spark Plasma Sintering. J Electron Mater, 2011, 40: 1100–1106.

14 Wang H, Sun X, Yan X, *et al.* Fabrication and thermoelectric properties of highly textured $Ca_9Co_{12}O_{28}$ ceramic. J Alloys Compds, 2014, 582: 294–298.

15 Sotelo A, Rasekh Sh, Constantinescu G, *et al.* Improvement of textured $Bi_{1.6}Pb_{0.4}Sr_2Co_{1.8}O_x$ thermoelectric performances by metallic Ag additions. Ceram Int, 2013, 39: 1597–1602.

16 Rasekh Sh, Ferreira NM, Costa FM, *et al.* Development of a new thermoelectric $Bi_2Ca_2Co_{1.7}O_x$ + $Ca_3Co_4O_9$ composite. Scr Mater, 2014, 80: 1–4.

17 Delorme F, Chen C, Pignon B, *et al.* Promising high temperature thermoelectric properties of dense $Ba_2Co_9O_{14}$ ceramics. J Eur Ceram Soc, 2017, 37: 2615–2620.

18 Constantinescu G, Rasekh Sh, Torres MA, *et al.* Effect of Sr substitution for Ca on the $Ca_3Co_4O_9$ thermoelectric properties. J Alloys Compds, 2013, 577: 511–515.

19 Delorme F, Martin CF, Marudhachalam P, *et al.* Effect of Ca substitution by Sr on the thermoelectric properties of $Ca_3Co_4O_9$ ceramics. J Alloys Compds, 2011, 509: 2311–2315.

20 Sotelo A, Rasekh Sh, Torres MA, *et al.* Effect of synthesis methods on the $Ca_3Co_4O_9$ thermoelectric ceramic performances. J Solid State Chem, 2015, 221: 247–254.

21 Chemistry WebBook of NIST. http://webbook.nist.gov/chemistry/

22 Woermann E, Muan A. Phase equilibria in the system CaO-cobalt oxide in air. J Inorg Nucl Chem, 1970, 32: 1455–1459.

23 Liu H, Lin GC, Ding XD, *et al*. Mechanical relaxation in thermoelectric oxide $Ca_{3-x}Sr_xCo_4O_{9+\delta}$ (x=0, 0.25, 0.5, 1.0) associated with oxygen vacancies. J Solid State Chem, 2013, 200: 305–309.

24 Delorme F, Diaz-Chao P, Guilmeau E, *et al.* Thermoelectric properties of $Ca_3Co_4O_9$–Co_3O_4 composites. Ceram Int, 2015, 41: 10038–10043.

25 Delorme F, Ovono Ovono D, Marudhachalam P, *et al.* Effect of precursors size on the thermoelectric properties of $Ca_3Co_4O_9$ ceramics. Mater Res. Bull, 2012, 47: 1169–1175.

26 Kahraman F, Madre MA, Rasekh Sh, *et al.* Enhancement of mechanical and thermoelectric properties of $Ca_3Co_4O_9$ by Ag addition. J Eur Ceram Soc, 2015, 35: 3835–3841.

27 Kenfaui D, Chateigner D, Gomina M, *et al*. Texture, mechanical and thermoelectric properties of $Ca_3Co_4O_9$ ceramics. J Alloys Compds, 2010, 490: 472–479.

28 Rasekh Sh, Torres MA, Constantinescu G, *et al.* Effect of Cu by Co substitution on $Ca_3Co_4O_9$ thermoelectric ceramics. J Mater Sci Mater Electron, 2013, 24: 2309–2314.

29 Schulz T, Topfer J. Thermoelectric properties of $Ca_3Co_4O_9$ ceramics prepared by an alternative pressure-less sintering/annealing method. J Alloys Compds, 2016, 659: 122–126.

30 Sotelo A, Costa FM, Ferreira NM, *et al.* Tailoring $Ca_3Co_4O_9$ microstructure and performances using a transient liquid phase sintering additive. J Eur Ceram Soc, 2016, 36: 1025–1032.

31 Li Y-N, Wu P, Zhang S-P, *et al.* Thermoelectric properties of lower concentration K-doped $Ca_3Co_4O_9$ ceramics. Chin Phys B, 2018, 27: 057201.

32 Zhang Y, Zhang J, Lu Q. Synthesis of highly textured $Ca_3Co_4O_9$ ceramics by spark plasma sintering. Ceram Int, 2007, 33: 1305–1308.

33 Noudem JG, Kenfaui D, Chateigner D, *et al.* Toward the enhancement of thermoelectric properties of lamellar $Ca_3Co_4O_9$ by edge-free spark plasma texturing. Scr Mater, 2012, 66: 258–260.

34 Koshibae W, Tsuitsui K, Maekawa S. Thermopower in cobalt oxides. Phys Rev B Condens Matter, 2000, 62: 6869–6872.

35 Tian R, Donelson R, Ling CD, *et al*. Ga substitution and oxygen diffusion kinetics in $Ca_3Co_4O_{9+\delta}$-based thermoelectric oxides. J Phys Chem, 2013, 32: 1455–1459.

Figure captions

Figure 1. Representative micrographs of the mixture of $CaCO_3$, $SrCO_3$, and CoO powders, after: a) mixing; b) ball milling at 300 rpm for 30 min; and c) attrition milling for 30 min.

Figure 2. FTIR spectra of different precursor powders: a) initial mixture; and after calcination processes: b) ball milled after 750 ºC for 12 h and 800 ºC for 12 h; and attrition milled after c) 800 ºC 1 h; d) 825 ºC 1 h; and e) 850 ºC 1 h.

Figure 3. Representative micrographs performed on calcined powders a) ball milled after 750 ºC 12 h, and 800 ºC 12 h; and b) attrition milled after 850 ºC 1 h.

Figure 4. Powder XRD patterns of Sr-doped textured $Ca_3Co_4O_9$ samples prepared from: a) ball; and b) attrition milled powders. The diffraction planes indicate the reflections associated to the $Ca_3Co_4O_9$ phase, while * identify those of $Ca_3Co_2O_6$ one.

Figure 5. Representative SEM micrograph performed on polished longitudinal sections of Sr-doped textured $Ca_3Co_4O_9$ samples prepared from: a) ball; and b) attrition milled powders. The arrows identify the $Ca_3Co_2O_6$ phase.

Figure 6: Representative SEM micrographs performed on fractured transversal sections of Sr-doped hot-pressed $Ca_3Co_4O_9$ samples prepared from a) ball; and b) attrition milled powders.

Figure 7: Temperature dependence of the electrical resistivity for Sr-doped $Ca_3Co_4O_9$ textured samples produced from ball milled (●); and attrition milled (■) powders.

Figure 8: Temperature dependence of the Seebeck coefficient for Sr-doped $Ca_3Co_4O_9$ textured samples produced from ball milled (●); and attrition milled (■) powders.

Figure 9: Temperature dependence of the power factor for Sr-doped $Ca_3Co_4O_9$ textured samples produced from ball milled (●); and attrition milled (■) powders.

Table 1: Density of both samples after hot-pressing, together with their standard errors; relative density using 4.677 g cm^{-3} as the theoretical one [6]; and maximum bending strength with its standard error.

Sample	Density (g cm^{-3})	Standard error	Relative density (%)	σ_{max} (MPa)	Standard error
CS	4.52	0.05	96.6	287	20
AT	4.50	0.06	96.2	212	5

Figure 1

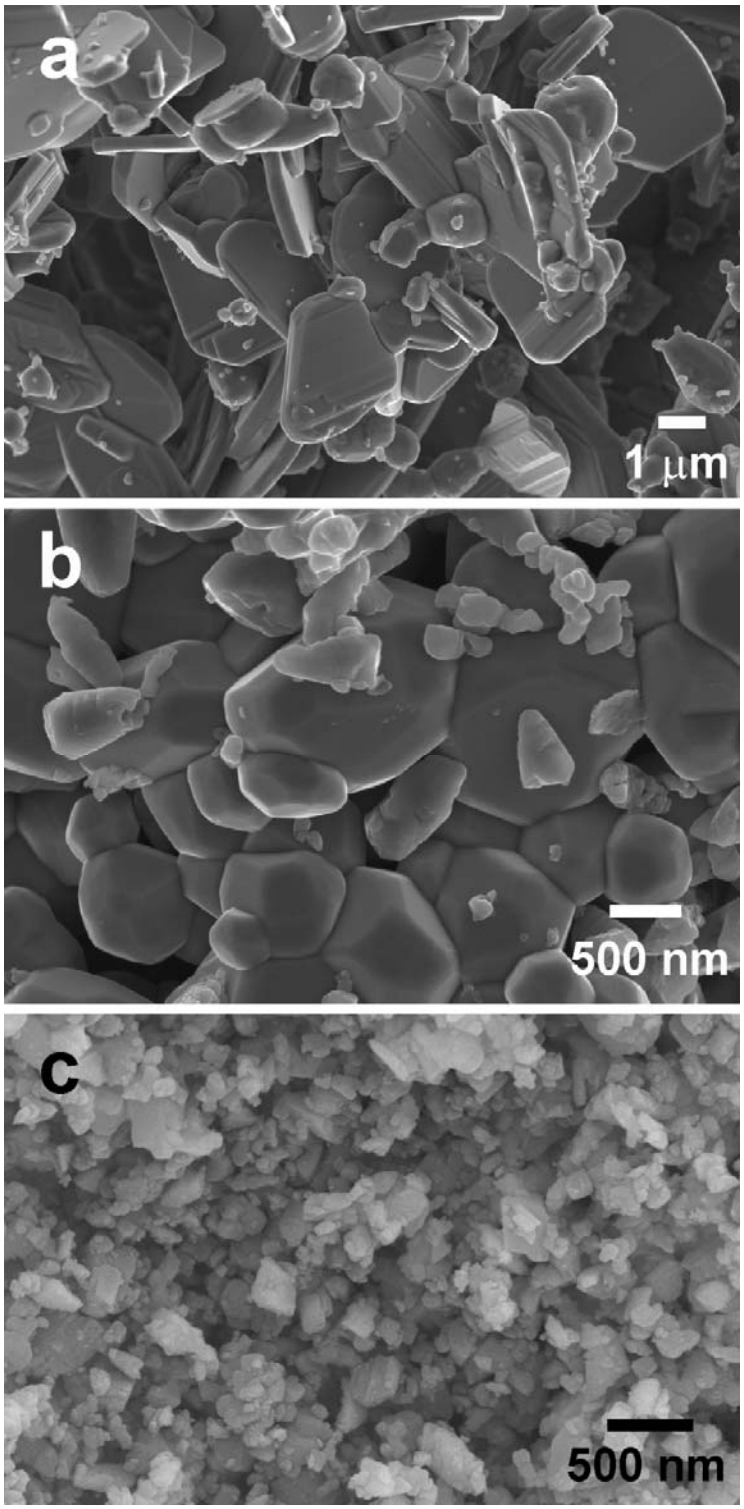

Figure 2

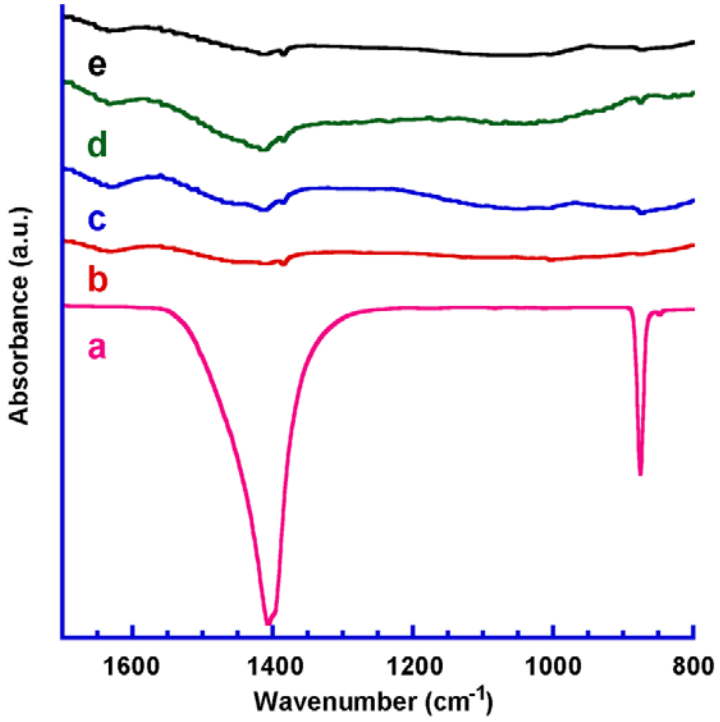

Figure 3

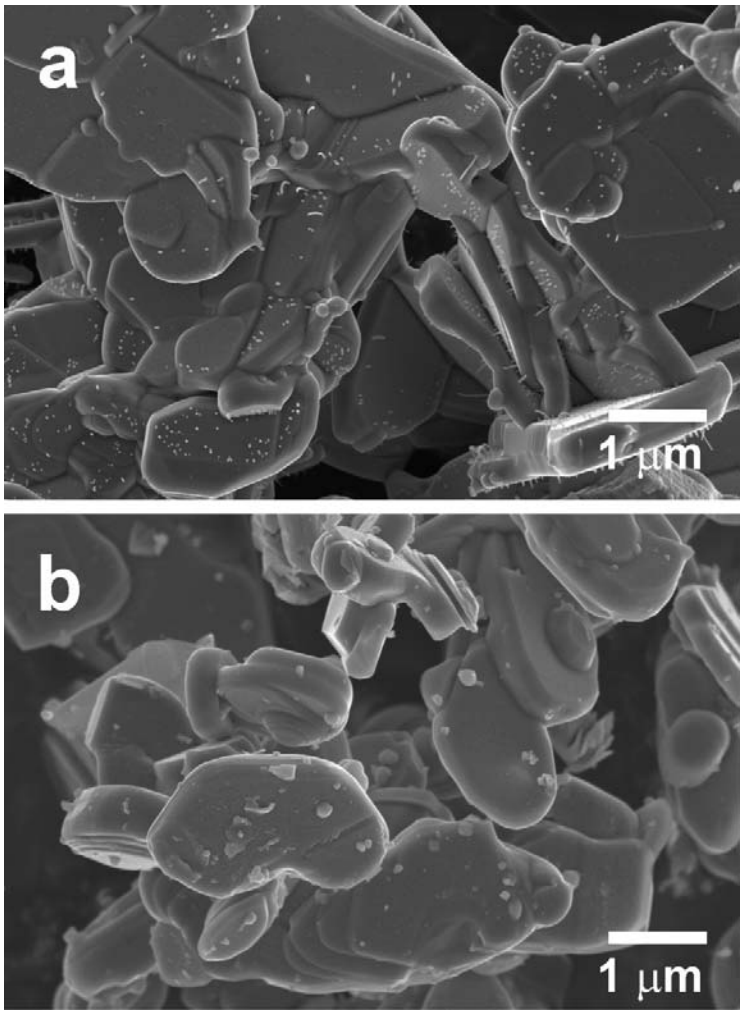

Figure 4

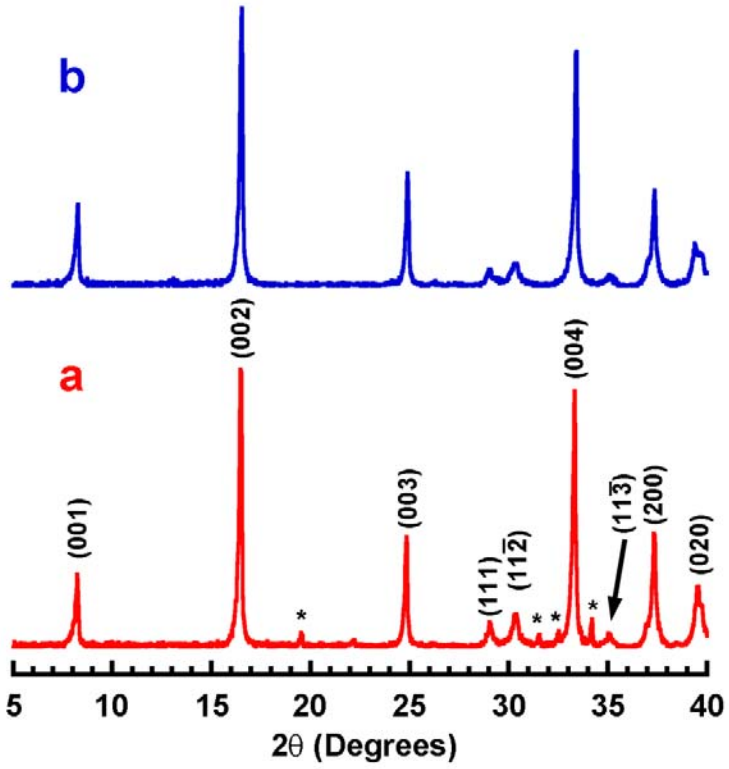
b
a
(001)
(002)
(003)
(111)
(11$\bar{2}$)
(004)
(11$\bar{3}$)
(200)
(020)
*
5
10
15
20
25
30
35
40
2θ (Degrees)

Figure 5

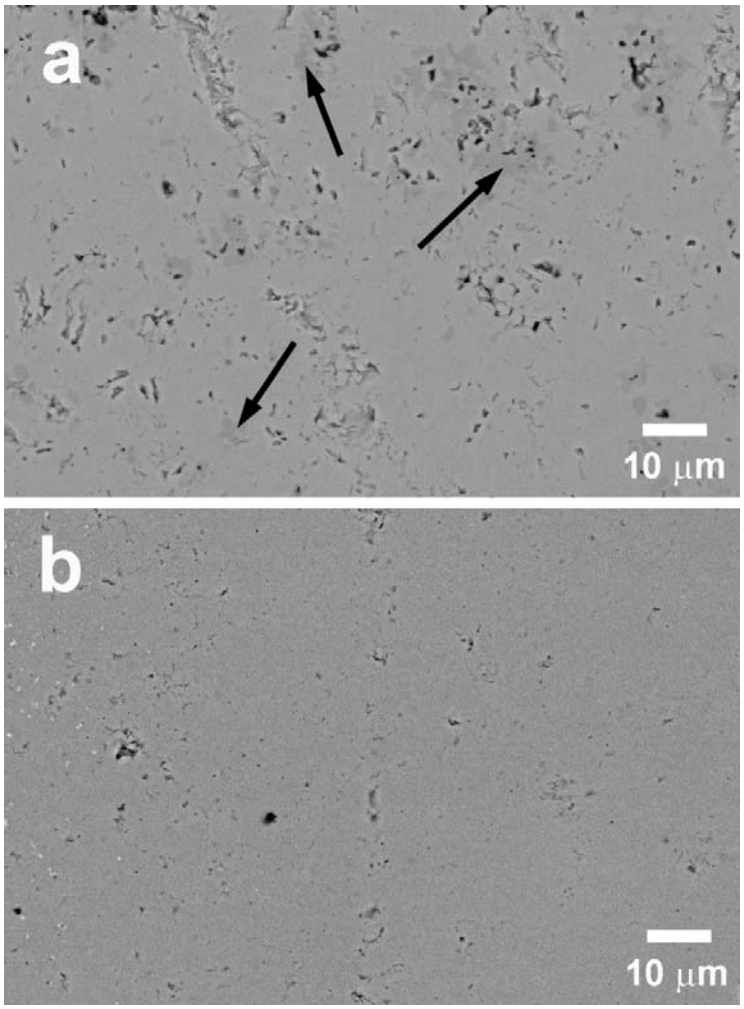

Figure 6

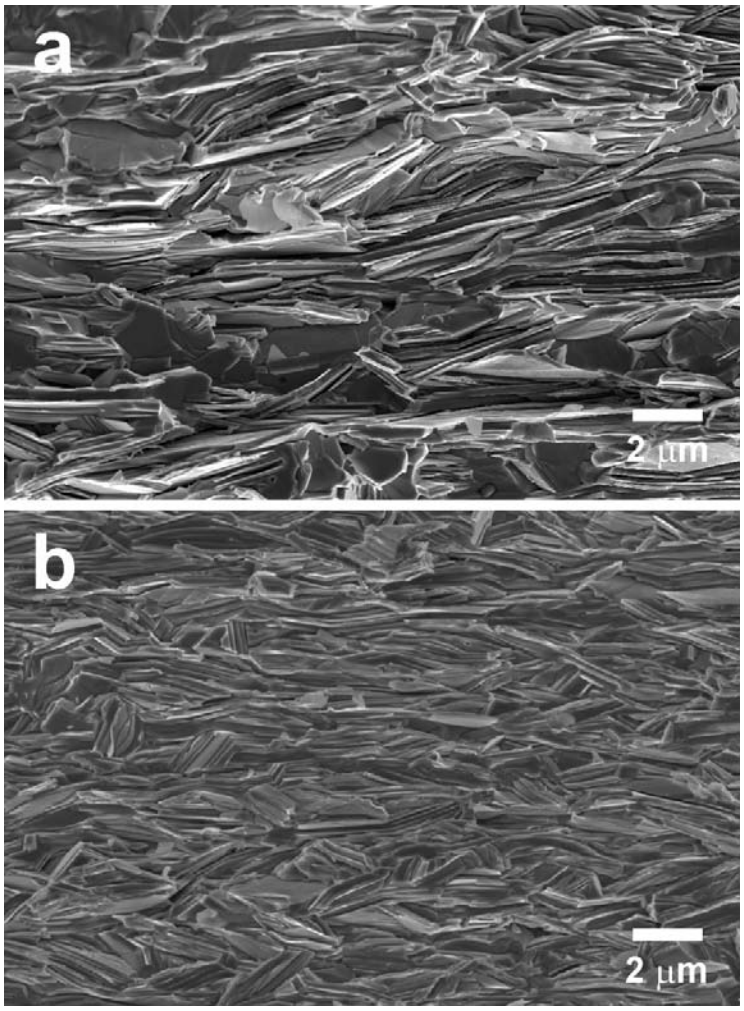

Figure 7

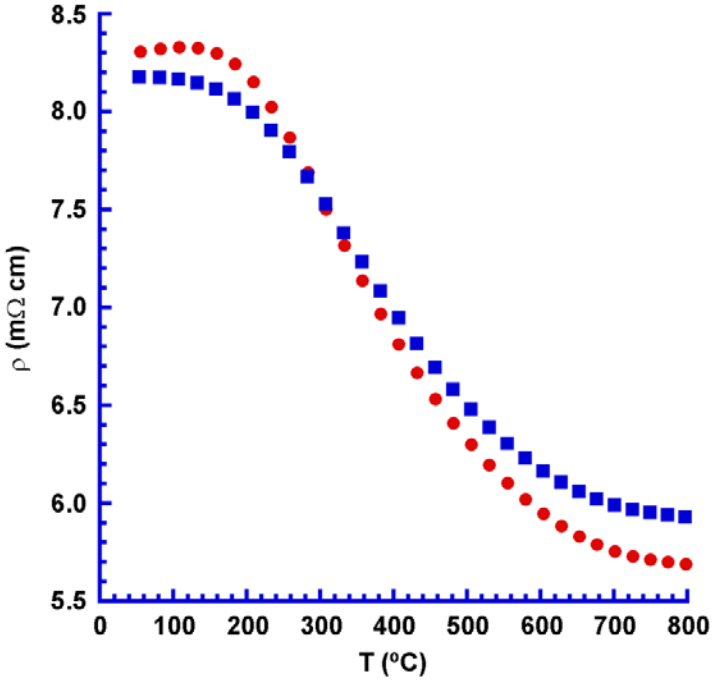

Figure 8

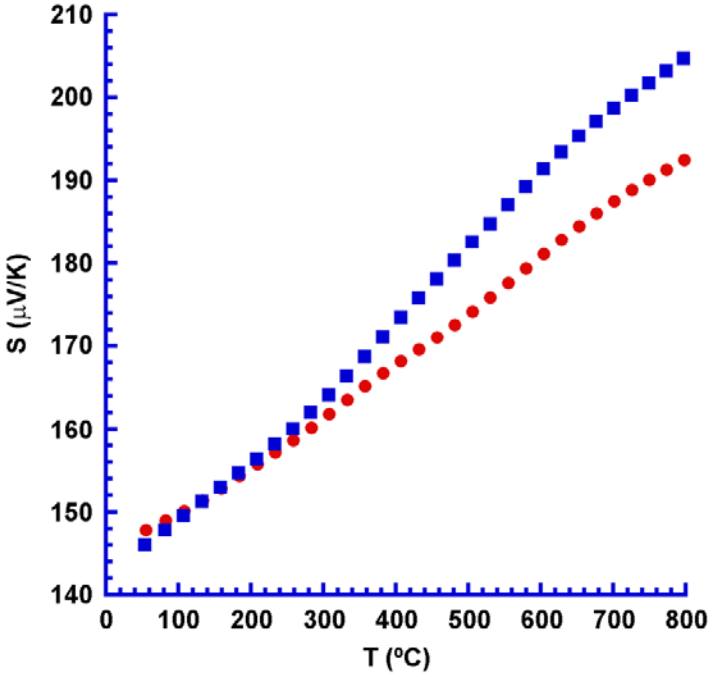
210
200
190
180
170
160
150
140
S (μV/K)
0
100
200
300
400
500
600
700
800
T (ºC)

Figure 9